3D-QSAR studies of 2,2-diphenylpropionates to aid discovery of novel potent muscarinic antagonists

Apurba K. Bhattacharjee [a,*], Jonathan A. Gordon [b,†], Elizabeth Marek [a], Amy Campbell [c], Richard K. Gordon [a]

[a] Department of Regulated Laboratories, Division of Regulated Activities, Walter Reed Army Institute of Research, Silver Spring, MD 20910, USA
[b] Richard Montgomery High School, Rockville, MD 20850, USA
[c] Division of Biochemistry, Walter Reed Army Institute of Research, Silver Spring, MD 20910, USA

ARTICLE INFO

ABSTRACT

Muscarinic acetylcholine receptors (mAChRs) consisting of five known subtypes, are widely distributed in both central and peripheral nervous systems for regulation of a variety of critical functions. The present theoretical study describes correlations between experimental and calculated molecular properties of 15 α-substituted 2,2-diphenylpropionate antimuscarinics using quantum chemical and pharmacophore generation methods to characterize the drug mAChR properties and design new therapeutics. The calculated stereoelectronic properties, such as total energies, bond distances, valence angles, torsion angles, HOMO–LUMO energies, reactivity indices, vibrational frequencies of ether and carbonyl moieties, and nitrogen atom proton affinity were found to be well correlated when compared with experimentally determined inhibition constants from the literature using three muscarinic receptor assays: [^{3}H]NMS receptor binding, α-amylase release from rat pancreas, and guinea pig ileum contraction. In silico predicted toxicity on rat oral LD_{50} values correlated well with the [^{3}H]NMS binding in N4TG1 cells and α-amylase release assays, but not the ileum contraction assay. Next, to explore the functional requirements for potent activity of the compounds, we developed a preliminary 3D pharmacophore model using the in silico techniques. The resulting model contained a hydrogen bond acceptor site on the carbonyl oxygen atom and a ring aromatic feature on one of the two aromatic rings in these compounds. This model was used as a template to search an in-house database for novel analogs. We found compounds equal in inhibition potency to atropine and, importantly, six not reported before as antimuscarinics. These results demonstrate that this QSAR approach not only provides a basis for understanding the molecular mechanism of action but a pharmacophore to aid in the discovery and design of novel potent muscarinic antagonists.

© 2009 Elsevier Ltd. All rights reserved.

1. Introduction

Organophosphorus (OP) compounds are widely used in agriculture as pesticides and have been deployed by terrorists as chemical warfare nerve agents.[1] These compounds are highly toxic, which is a result of inhibition of the enzyme acetylcholinesterase (AChE). AChE hydrolyzes the neuron-mediator acetylcholine (ACh) at the synaptic clefts. Inhibition of AChE results in a build up of ACh, yields a cholinergic crisis, and can ultimately lead to death.[2] To counter the effects of OP poisoning, anticholinergics (as functional drugs), and AChE reactivators (as causal drugs) are generally used as first aid antidotes.[2–5] Although present treatments for OP intoxication offer protection against their lethality, convulsions and behavioral consequences are not completely prevented. Muscarinic receptors (mAChR) have been widely used as targets of drug treatments for OP poisoning as this receptor becomes over stimulated due to accumulation of ACh (cholinergic overload). By agonist and antagonist evaluation[6] and molecular dissection,[7] five subtypes of muscarinic receptors have been determined, namely M1, M2, M3, M4, and M5. However, lack of small molecule ligands to inhibit muscarinic receptor subtypes selectively remains a major obstacle not only for better understanding of the role of the subtypes but also toward development of novel antimuscarinic therapeutics.[6]

Although several muscarinic agonists and antagonists have been recently approved for a variety of clinical conditions that include glaucoma, gastrointestinal and urinary bladder smooth-muscle disorders, bronchial asthma, peptic ulcers, Sjogren's syndrome, certain forms of cardiac arrhythmias, motion sickness, and Parkinson's disease,[8] the usefulness of these agents is frequently compromised due to side effects by non-selective

* Corresponding author. Tel.: +1 301 319 9043; fax: +1 301 319 9070.
E-mail address: Apurba.Bhattacharjee@amedd.army.mil (A.K. Bhattacharjee).
† Present address: Whiting School of Engineering, Johns Hopkins University, Baltimore, MD 21218, USA.

activation or blockade of multiple muscarinic receptor subtypes. Drugs that possess multiple protective functions such as exhibiting both reversible antimuscarinic activity (as observed for atropine) and reversible anticholinesterase (in place of pyridostigmine bromide) properties might be of unusual utility and efficacy for organophosphate poisoning, simultaneously protecting AChE from an irreversible OP inhibition and the occupation of muscarinic receptors by accumulated acetylcholine.[9] The pyridophens consisted of the basic pyridostigmine skeleton to carbamylate acetylcholinesterase combined with the 2,2-diphenylpropionate portion of aprophen by replacement of the diethylamino group. The resulting pyridophens exhibited less potent antimuscarinic activity of aprophen but showed some specificity in inhibiting acetylcholinesterase preferentially in comparison with butyrylcholinesterase. Another scenario would be the use of oximes that also possess antinicotinic receptor or antimuscarinic properties in addition to the oxime moiety to reactivate non-aged organophosphate inhibited cholinesterases. Tattersall[10] described the moderate protection afforded by a series of mono- and bis-oximes by interaction with nicotinic acetylcholine receptor ion channels and demonstrated this affect in the absence of cholinesterase reactivation. In another example, Loke et al.[11,12] demonstrated antimuscarinic properties of pralidoxime (a mono-oxime) derivatives that lacked appreciable reactivation activity, although pralidoxime has been reported previously to be an antimuscarinic in receptor binding assays.[13] Taken together, optimization of drugs for interaction at muscarinic receptors specifically and cholinergic receptors in general may provide more efficacious therapeutics for organophosphate poisoning.

There are efforts for discovery and design of new antagonists targeting a subtype-specific mAChR, for example, to treat overactive bladder or ocular diseases.[6] Discovery and development of new therapeutics are expensive and complex processes. It takes almost 10 years and an average $500 million to bring a new therapeutic agent from the bench of discovery to the market.[14] Thus, newer technologies that can improve the efficiency of the discovery process are indeed valuable to the pharmaceutical industry.[14,15]

Computer-assisted molecular modeling (CAMM) evolved to enable advances in mechanistic drug design and in the discovery of new potential bioactive chemical entities.[15,16] The current advances in the in silico methodologies allow direct applications ranging from accurate ab initio quantum chemical calculations of stereoelectronic properties, generation of three-dimensional pharmacophores, and performance of database searches to identify potent bioactive agents. Thus, quantitative structure–activity relationship (QSAR) studies using quantum chemical and pharmacophore generation methods on known antagonists should provide important molecular level information to aid in the discovery and custom design of new therapeutics. In continuation of our efforts to design and discover new therapeutics from three dimensional quantitative structure–activity relationship studies[17–19] and to better understand the molecular mechanism of action of bioactive agents,[20] we present here a detailed QSAR study on stereoelectronic and pharmacophoric properties of 15 reported [3] α-substituted 2,2-diphenylpropionate antimuscarinic agents. Semi-empirical (AM1-Austin Model 1)[21] and ab initio (RHF/B3LYP/6-31G** basis set) quantum chemical methods[22] were used in a graduated manner followed by pharmacophore generation using the CATALYST methodologies. The overall objectives were: (a) to better understand the molecular mechanism of antagonistic activity of the compounds, (b) to develop a pharmacophore model for antagonist activity of the compounds, (c) to use the model for successful identification of unknown muscarinic antagonists, and (d) to provide a basis for designing more efficacious drugs for binding to muscarinic receptors. In the future, the novel antagonists will be evaluated for subtype selectivity, and refinement of the pharmacophore to predict characteristics which define the five receptor types.

2. Results and discussion

Structures of the 2,2-diphenylpropionate antimuscarinic agent (see Ref. 3, Gordon et al.) used in this study are presented in Chart 1. The IUPAC names of the compounds are 3-(2,2-diphenylpropanoyloxy)-1-ethylpiperidinium **1**, 2-((2,2-diphenylpropanoyloxy)methyl)-1-methylpiperidinium **2**, 3-(2,2-diphenylpropanoyloxy)-1-methylpyrrolidinium **3**, 1-(2-(2,2-diphenylpropanoyloxy)ethyl)pyrrolidinium **4**, 3-(2,2-diphenylpropanoyloxy)-1-azoniabicyclo[2.2.2]octane **5**, (3R,8R)-3-(2,2-diphenylpropanoyloxy)-8-methyl-8-azoniabicyclo[3.2.1]octane **6**, 1-(2-(2,2-diphenylpropanoyloxy)ethyl)piperidinium **7**, 3-((2,2-diphenylpropanoyloxy)methyl)-1-methylpiperidinium **8**, (7S)-7-(2,2-diphenylpropanoyloxy)-2-methyl-2-azoniabicyclo[3.3.1]nonane **9**, 2-(2-(2,2-diphenylpropanoyloxy)ethyl)-1-methylpyrrolidinium **10**, (1s,4s)-4-(2,2-diphenylpropanoyloxy)-1-ethylpiperidinium **11**, (1s,4s)-4-(2,2-diphenylpropanoyloxy)-1-ethylpiperidinium **12**, (3R)-3-(2,2-diphenylpropanoyloxy)-6-methyl-6-azoniabicyclo[3.2.1]octane **13**, 4-((2,2-diphenylpropanoyloxy)methyl)-1-methylpiperidinium **14**, 4-((2,2-diphenylpropanoyloxy)methyl)-1-ethylpiperidinium **15**, and (1R,3r,5S)-8-methyl-8-azabicyclo[3.2.1]octan-3-yl 3-hydroxy-2-phenylpropanoate (atropine).

Modeling and simulations performed on the α-substituted 2,2-diphenylpropionates (**1–15**) and atropine (Chart 1) showed several interesting trends of correlation with the experimental antimuscarinic activity of the agents. Results and discussions on these theoretical calculations and correlations are presented below:

2.1. Optimized geometry in vacuum

The geometry of all 15 2,2-diphenylpropionates and atropine were fully optimized first using molecular mechanics and subsequently by semi-empirical AM1 and ab initio quantum chemical methods following the hierarchy of basis sets and optimally choosing B3LYP/6-31G** for all calculations. The ab initio B3LYP/6-31G** optimized geometry of the α-substituted 2,2-diphenylpropionate antimuscarinic agents are shown in Figure 1. Calculated bond distance between the carbonyl oxygen and protonated nitrogen atom of heterocyclic ring and the torsion angle between atoms connecting the heterocyclic ring and the two aromatic rings were found to correlate with [³H]NMS binding pK_i inhibition values; bond distance showed a parabolic relationship with the pK_i constants consistent with the previously reported observation[3] (Fig. 2). In contrast, the torsion angles showed a tendency for a linear relationship (r^2 = 0.7) with the experimental binding (Fig. 3). Ab initio quantum chemical B3LYP/6-31G** calculations are reported in Tables 1 and 2. A few of the structural parameters calculated using the semi-empirical AM1 calculations are shown in Table 3.

2.2. Geometry in aqueous medium

Solvent is critical in the determination of thermodynamics and kinetics of chemical reactions.[23] Thus, to investigate the interactive abilities of compounds in physiological conditions, we performed simulations in aqueous phase using semi-empirical AM1 calculations and quantum chemical single point polarizable continuum (PCM) aqueous solvation calculations using B3LYP/6-31G**/SCRF = PCM theory. Although ab initio QM results demonstrated a consistent aqueous stabilization for all the compounds ranging between 51.0 and 37.0 kcal/mol (Table 1), no correlation with biological activity was observed. However, it is notable that neutral atropine is found to be stabilized by only 9 kcal/mol in aqueous medium whereas the protonated atropine is stabilized by
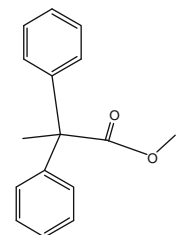
| #	Structure	pK$_i$ (M)	#	Structure	pK$_i$ (M)
1		6.3±0.03	9		8.3±0.06
2		6.8±0.06	10		8.0±0.06
3		7.8±0.04	11		8.8±0.04
4		8.2±0.04	12		9.0±0.04
5		8.2±0.02	13		8.3±0.04
6		8.4±0.02	14		7.7±0.02
7		8.2±0.02	15		6.9±0.06
8		7.8±0.03	Atr		8.7±0.08

Atr = atropine.

Chart 1. Structures of the 2,2-diphenylpropionate antimuscarinic agent (see Ref. 3, Gordon et al.). (Compound numbers are indicated as #.)

51 kcal/mol in water (Table 1). To obtain further insight of the solubility process, complete geometry optimization of each of the compounds was carried out as a solute in periodic boxes filled with water molecules using AM1 quantum chemical calculations. The
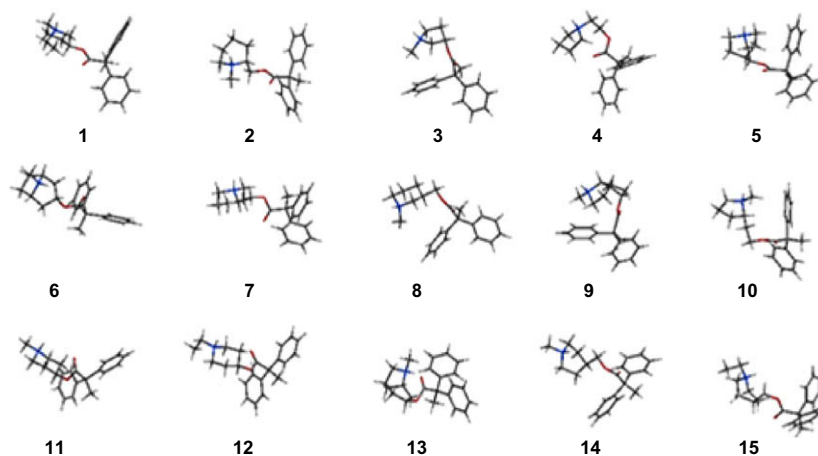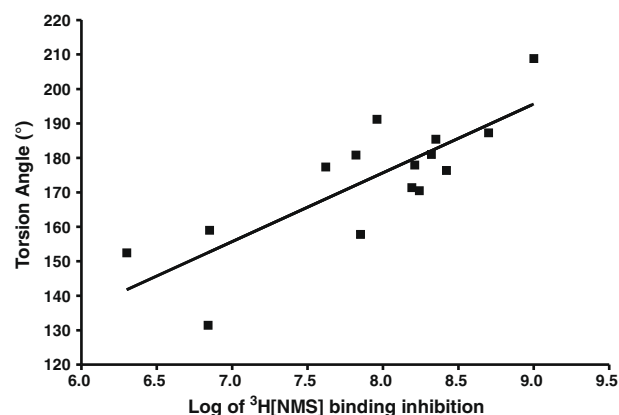
Figure 1. B3LYP-6-31G** optimized structures of α-substituted 2,2-diphenylpropionate antimuscarinics. (Color of atoms: C = grey, O = red, protonated N and N = blue, and H = white.)
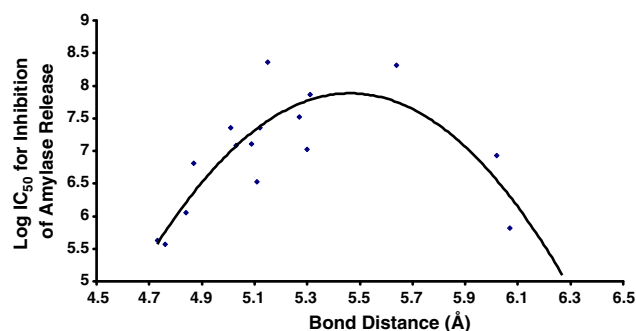
Figure 2. Parabolic relationship established between the bond distance (carbonyl oxygen and protonated nitrogen) (x-axis) and log IC$_{50}$ values for inhibition of amylase release (y-axis).

Figure 3. Linear relationship (r^2 = 0.7) established between log ^{3}H [NMS] binding inhibition (x-axis) and torsion angle (between atoms connecting the heterocyclic ring and the two aromatic rings (y-axis).

activity of the compounds was found to decrease with increasing number of water molecules implying the role of dilution in decreasing the inhibition potency of the compounds. The study was continued using boxes of five different sizes with edge of 13 Å, 18 Å, 23 Å, 28 Å, and 33 Å with the individual compounds

followed by complete optimization of each of the boxes. Results showed that as the compounds are placed in larger boxes with water, energies decrease significantly (Table 4). Calculated ΔG_{aq}

Table 1
Absolute energies (in hartrees) of the 2,2-diphenylpropionates **1–15**, atropine (neutral), and atropine (protonated) obtained by geometry optimization performed at B3LYP/6-31G** theory level (DFT ab initio quantum chemical methods)

Compound#	Total energy in vacuo (in hartrees)*	Total energy in aqueous medium (in hartrees)*	Relative energies (kcal/mol)	ΔG (aqueous solvation) (kcal/mol)	[^{3}H]NMS binding, pK_i (experimental)[3] (M)
1	−1060.2410556	−1060.316933	47.4	−49.34	6.3 ± 0.03
2	−1060.225409	−1060.299809	46.7	−47.49	6.8 ± 0.06
3	−981.601601	−981.681738	50.3	−51.08	7.8 ± 0.04
4	−1020.913624	−1020.989113	47.3	−48.73	8.2 ± 0.04
5	−1059.026154	−1059.103347	48.4	−50.23	8.2 ± 0.02
6	−1098.334489	−1098.409927	47.3	−51.36	8.4 ± 0.02
7	−1060.19344	−1060.27081	48.5	−47.96	8.2 ± 0.02
8	−1099.553522	−1099.630206	48.1	−47.21	7.8 ± 0.03
9	−1098.347235	−1098.422869	47.4	−47.52	8.3 ± 0.06
10	−1060.231888	−1060.30897	48.3	−45.37	8.0 ± 0.06
11	−1020.920199	−1021.001038	50.7	−52.89	8.8 ± 0.04
12	−1060.239443	−1060.316669	48.4	−50.54	9.0 ± 0.04
13	−1098.353763	−1098.413733	37.6	−40.9	8.3 ± 0.04
14	−1060.220564	−1060.301978	51.1	−53.62	7.7 ± 0.02
15	−1099.539801	−1099.618114	49.1	−50.91	6.9 ± 0.06
Atropine	−902.772245	−902.786423	8.9	−8.76	8.7 ± 0.08
Atropine-protonated	−903.164305	−903.245818	51.1	−54.79	NA**

*1 hartree = 627.5 kcal/mol. NA**(pK_i for atropine-protonated) = not available.

A. K. Bhattacharjee et al. / Bioorg. Med. Chem. 17 (2009) 3999–4012

4003

Table 2
Stereoelectronic parameters for the optimized structures of 2,2-diphenylpropionates **1–15**, atropine (neutral), and atropine (protonated) calculated at B3LYP/6-31** theory levels along with their experimental efficacy data

Compound#	[3H]NMS binding, pK_i (expt.)[3] (M)	Distance (Å) (carbonyl O– protonated N)	Torsion angles (°) (heterocyclic ring and the two aromatic rings)	Negative potential (C=O) (kcal/ mol)	Positive potential (N+) (kcal/mol)	Gap (HOMO– LUMO) (eV)	Charges (electrons) (at B3LYP/6-31G**) O (C=O)	Charges (electrons) (at B3LYP/6-31G**) N
1	6.3 ± 0.03	4.73	152.491	16.8	149.8	5.29	−0.488	−0.45
2	6.8 ± 0.06	4.76	158.984	23.6	150.1	5.23	−0.493	−0.465
3	7.8 ± 0.04	4.84	157.835	18.7	153.5	5.12	−0.47	−0.112
4	8.2 ± 0.04	4.87	171.375	25.8	150.5	5.32	−0.493	−0.122
5	8.2 ± 0.02	5.01	170.515	16.8	150.6	5.23	−0.477	−0.124
6	8.4 ± 0.02	5.03	176.381	10.9	147.5	5.06	−0.48	−0.115
7	8.2 ± 0.02	5.09	177.936	16.9	149.3	5.31	−0.474	−0.111
8	7.8 ± 0.03	5.11	180.872	9.72	148.3	5.45	−0.578	−0.39
9	8.3 ± 0.06	5.15	185.452	13.7	145.7	5.29	−0.468	−0.119
10	8.0 ± 0.06	5.27	191.226	15.5	148.3	5.37	−0.474	−0.111
11	8.8 ± 0.04	5.30	187.274	15.1	149.8	5.07	−0.498	−0.096
12	9.0 ± 0.04	5.31	208.837	14.3	146.7	5.27	−0.499	−0.1
13	8.3 ± 0.04	5.64	181.027	26.6	112.8	5.16	−0.55	−0.078
14	7.7 ± 0.02	6.02	177.384	10.3	151.9	5.07	−0.565	−0.388
15	6.9 ± 0.06	6.07	131.474	9.25	148.9	5.23	−0.566	−0.397
Atropine	8.7 ± 0.08	5.12	NC*	−40.7	39.0	5.52	−0.509	−0.288
Atropine (protonated)	NA**	4.98	NC*	16.2	150.1	5.78	−0.582	−0.476

NA**(pK_i for atropine-protonated) = not available. NC* = not calculated due to structure difference.

Table 3
Structural parameters for the optimized geometry of 2,2-diphenylpropionates **1–15**, atropine (neutral), and atropine (protonated) calculated using semi-empirical methods along with their experimental efficacy data

Compound#	Carbonyl oxygen stretching frequency (cm^{-1})	Ether oxygen stretching frequency (cm^{-1})	Rat oral LD$_{50}$ (mg/kg)	Log P	[3H]NMS binding, pK_i (expt.)[3] (M)
1	2109.1	1441.25	369.0	4.54	6.3 ± 0.03
2	2157.52	1473.92	264.0	4.62	6.8 ± 0.06
3	2172.61	1534.73	134.8	3.92	7.8 ± 0.04
4	2173.45	1541.01	253.9	4.22	8.2 ± 0.04
5	2171.74	1556.87	175.8	4.09	8.2 ± 0.02
6	2149.25	1548.58	74.2	4.48	8.4 ± 0.02
7	2168.43	1541.78	272.9	4.64	8.2 ± 0.02
8	2186.74	1528.15	109.3	4.83	7.8 ± 0.03
9	2152.89	1561.83	208.6	4.35	8.3 ± 0.06
10	2175.73	1533.13	123.9	4.48	8.0 ± 0.06
11	2119.69	1568.21	147.3	4.20	8.8 ± 0.04
12	2111.24	1573.19	45.6	4.54	9.0 ± 0.04
13	2157.16	1560.24	180.2	4.35	8.3 ± 0.04
14	2168.46	1509.14	287.6	4.36	7.7 ± 0.02
15	2155.72	1473.79	246.0	4.69	6.9 ± 0.06
Atropine	NC*	NC*	602.7	0.80	8.7 ± 0.08
Atropine (protonated)	NC*	NC*	2100.0	0.44	NA**

NC* = not calculated due to structure difference.
NA**(pK_i for atropine-protonated) = not available.

values using the ab initio polarizable continuum model (Table 1) were consistent with the above results, that is, greater aqueous solvation of the protonated dipropionates and protonated atropine compared to neutral atropine. Thus, water molecules play an important role in the interaction of these compounds with the muscarinic receptor.

2.3. Calculated infrared spectral analysis

Since bond-flexibility is an important characteristic of a molecule which can be reasonably assessed by infra red spectral analysis, we calculated the vibration frequencies of the structures and analyzed the spectrum for each of the 15 compounds and atropine using the semi-empirical AM1 method. Three significant stretching vibrations having large intensities were identified. The α-substituted 2,2-diphenylpropionate antimuscarinic agents: ether, carbonyl, and the protonated nitrogen atom in the heterocyclic ring in the compounds. The calculated frequencies of vibrations (Table 3) were plotted against the three experimentally determined activity values [3H]NMS binding, amylase secretion, and ileum contraction. The frequency of the carbonyl oxygen stretching when plotted against the [3H]NMS binding affinity followed a linear trend with a quadratic equation, $y = -40.111x^2 + 611.67x - 152.93$. The correlation coefficient observed was 0.92 (Fig. 4, Table 3). However, ether oxygen stretching varied linearly with the binding affinity with a correlation coefficient of 0.80 (Fig. 5, Table 3). But the frequency of the protonated nitrogen atom in the heterocyclic ring in the compounds did not correlate with experimental activity (not shown). These calculations suggest that the vibration frequency of two of the three observed large vibrational intensities, the carbonyl and the ether oxygen stretching, have important roles for the antimuscarinic activity of the compounds.

Table 4
Simulation of 2,2-diphenylpropionates **1–15** in water with different box sizes using AM1 and AM1 aq quantum chemical calculations (Compound numbers are indicated as #)

#	Box sizes (Å)	Number of water molecules	Energy with water (kcal/mol)	Energy without water (kcal/mol)
1	13	73	−72.868	19.26
	18	193	−435.73	18.83
	23	377	−1042.64	20.95
	28	725	−1779.18	98.99
	33	1187	−3062.43	101.87
2	13	73	−43.66	20.76
	18	193	−443.7	19.95
	23	377	−12.5	19.604
	28	725	−1866.46	19.501
	33	1187	−3148.38	19.07
3	13	73	−50.117	36.01
	18	193	−419.17	32.41
	23	377	−944.14	32
	28	725	−1858.09	31.98
	33	1187	−3127.81	31.96
4	13	73	−64.43	29.98
	18	193	−432.16	26.75
	23	377	−960.6	25.64
	28	725	−1864.62	25.38
	33	1187	−3138.27	25.26
5	13	73	−59.25	32.15
	18	193	−428.6	27.5
	23	377	−940.57	26.33
	28	725	−1854.94	26.18
	33	1187	−3099.43	25.97
6	13	73	−45.89	32.94
	18	193	−414.26	29.04
	23	377	−941.03	28.54
	28	725	−1850.08	28.41
	33	1187	−3127.43	28.29
7	13	73	−65.13	24.21
	18	193	−429.64	21.09
	23	377	−962.24	20.77
	28	725	−1865.31	20.45
	33	1187	−3143.5	19.85
8	13	73	−62.71	27.4
	18	193	−299.77	26.76
	23	377	−752.48	26.31
	28	725	−1572.89	26.08
	33	1187	−2904.87	25.97
9	13	73	−69.91	24.91
	18	193	−437.81	22.9
	23	377	−984.72	22.67
	28	725	−1904.38	22.51
	33	1187	−3279.18	22.39
10	13	73	−70.84	26.84
	18	193	−441.28	26.02
	23	377	−996.13	25.86
	28	725	−1917.17	25.72
	33	1187	−3385.14	25.63
11	13	73	−67.32	25.88
	18	193	−446.54	25.37
	23	377	−987.81	25.19
	28	725	−1940.43	25.03
	33	1187	−3297.73	24.93
12	13	73	−65.28	25.81
	18	193	−442.37	25.26
	23	377	−980.25	25.1
	28	725	−1921.76	24.98
	33	1187	−3241.87	24.89
13	13	73	−63.42	25.72
	18	193	−437.04	25.41
	23	377	−957.21	25.23
	28	725	−1892.47	25.06
	33	1187	−3194.77	24.99
14	13	73	−63.27	25.49
	18	193	−436.41	25.17

Table 4 (*continued*)

#	Box sizes (Å)	Number of water molecules	Energy with water (kcal/mol)	Energy without water (kcal/mol)
23	377	−955.18	25.02	
28	725	−1881.12	24.93	
33	1187	−3178.59	24.88	
15	13	73	−62.93	24.84
	18	193	−431.82	24.47
	23	377	−938.51	24.12
	28	725	−1817.47	23.92
	33	1187	−3121.45	23.83

2.4. Electronic property analysis

To obtain additional insight of the electronic properties of α-substituted 2,2-diphenylpropionates and atropine, the molecular electrostatic potential (MEP) profiles, molecular orbital energies, and reactivity indexes (difference between the HOMO, highest occupied molecular orbital and LUMO, lowest unoccupied molecular orbital energies) were calculated using the B3LYP/6-31G** density functional theory on the optimized geometry of the molecules. Calculated electrostatic potentials and the reactivity indexes of the compounds are reported in Table 2. Molecular electrostatic potential mapped onto the total electron density surface of each of the compounds is shown in Figure 6. The MEP profiles indicate that the most positive potential site (deepest blue) in all the compounds is, as expected, located around the positively charged nitrogen atom in the heterocyclic ring. Although no nega-
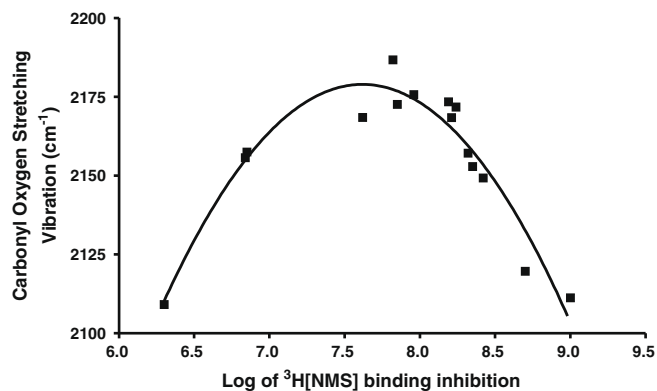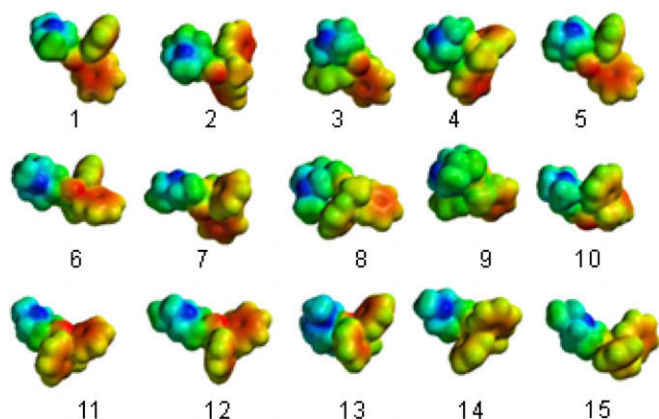

Figure 4. A plot showing a Quadratic relationship (r^2 = 0.92) observed between log 3H[NMS] binding inhibition (*x*-axis) and carbonyl oxygen stretching frequencies (*y*-axis).
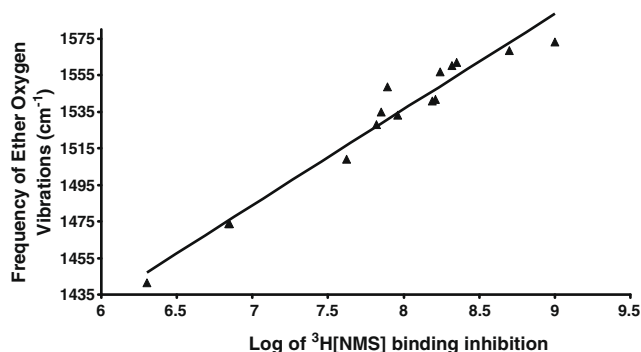
Figure 5. A plot showing a linear relationship between log 3H[NMS] binding inhibition (*x*-axis) and ether oxygen stretch (*y*-axis).

Figure 6. Molecular electrostatic potential (calculated at B3LYP/6-31G** level) isodensity surfaces of the α-substituted 2,2-diphenylpropionate antimuscarinics.

tive potential region is found in these compounds, the position by the carbonyl oxygen atom extending toward the aromatic ring through the ether oxygen atom is found to be consistently less positive (shown in red with varying intensity, Fig. 6). Red regions with decreasing intensity in the MEP profiles of the compounds indicate weak positive electrostatic potential regions, most notably regions at the aromatic rings in all the molecules, implying a hydrophobic nature of the aromatic rings. Since this feature is observed consistently in all the compounds, it is likely required for antimuscarinic activity.

The reactivity indexes (Gap, eV) of the compounds were calculated from the molecular orbital energies and are presented in Table 2. All were found to be within a narrow range of 5.06–5.52 eV (Table 2), indicating essentially a similar reactive nature of the compounds. These reactivity indexes are consistent with the observation of carbonyl oxygen and protonated nitrogen atoms in the structures. Three dimensional HOMO and LUMO isosurfaces over the van der Waals surface and the orbitals are

shown in Figures 7 and 8, respectively. In the HOMO isodensity surface of the molecules, the predominant HOMO is consistently observed on the aromatic ring of the compounds (Fig. 7), whereas in the LUMO profiles (Fig. 8), the most significant and the largest LUMO is consistently found to be localized by the protonated nitrogen atom in the heterocyclic ring of all the compounds. These features indicate strong nucleophilic affinity (LUMO) of the protonated nitrogen atom of the heterocyclic ring and electronic distribution (HOMO) by the aromatic ring. Both these features appear to be consistent with the MEP profiles and are likely to be important for potent activity of the compounds.

2.5. Comparison with atropine

In order to compare the theoretical data with a known standard, similar studies were performed using atropine and correlations between the calculated and experimental data were evaluated. No trends were observed with neutral atropine. But notably, when the nitrogen atom in atropine was protonated, several of the above mentioned calculated QSAR trends on the α-substituted 2,2-diphenylpropionate antimuscarinic compounds were found to be re-established. The protonated atropine exhibited a large positive electrostatic potential region by the nitrogen atom and the most dominant HOMO was located by the aromatic ring similar to the α-substituted 2,2-diphenylpropionates (Figs. 9 and 10). At physiological pH, the compounds are expected to be protonated. However, the LUMO characteristics and the reactivity indexes of both the neutral form and the protonated atropine appear to be similar (Fig. 11) (Table 2). The LUMO characteristics of protonated and neutral atropine clearly indicate that the reactive center is located around the carbonyl and hydroxyl moieties of the two species (Fig. 11). Electrostatic potential maps beyond the van der Waals surface for the neutral atropine (Fig. 12) are consistent with this observation. Calculated log P values of atropine and its protonated form are small compared to the 15 α-substituted 2,2-diphenylpropionate antimuscarinic agents (Table 3).
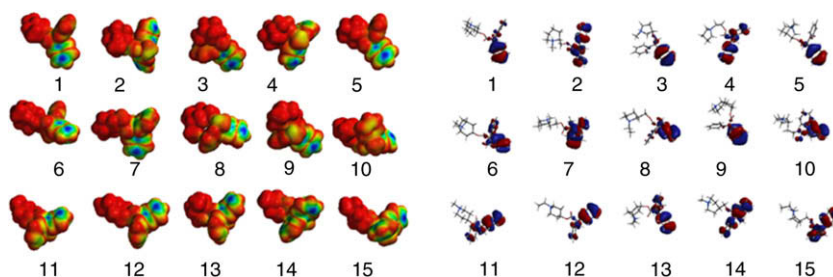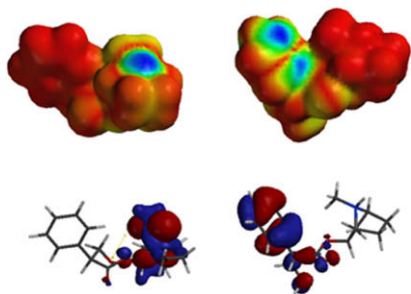

Figure 7. HOMO profiles (at B3LYP/6-31G** level) of the α-substituted 2,2-diphenylpropionate antimuscarinics. HOMO isodensity surfaces (left); HOMO dynamic surfaces (right).
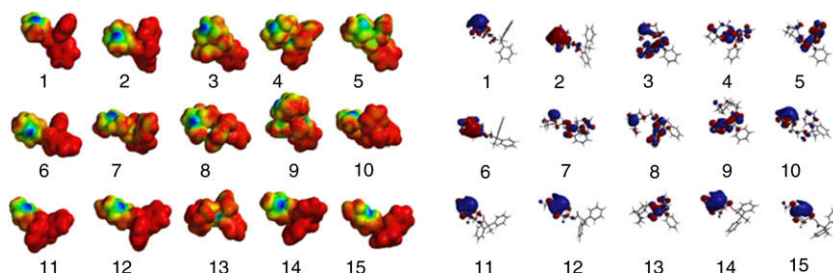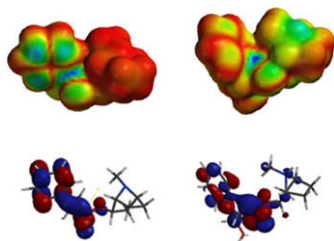

Figure 8. LUMO profiles (at B3LYP/6-31G** level) of the α-substituted 2,2-diphenylpropionate antimuscarinics. LUMO isodensity surfaces (left); LUMO dynamic surfaces (right).
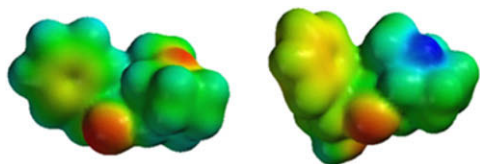
Figure 9. Molecular electrostatic potential isodensity surface (calculated at B3LYP/6-31G** level) of atropine (left) and protonated atropine (right).
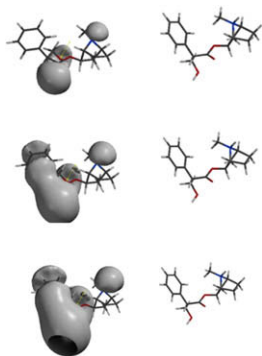

Figure 10. HOMO profiles (calculated at B3LYP/6-31G** level)) of atropine (left) and protonated atropine (right).


Figure 11. LUMO profiles (calculated at B3LYP/6-31G** level) of atropine (left) and protonated atropine (right).

2.6. In silico toxicity evaluation

In silico toxicity of the α-substituted 2,2-diphenylpropionate antimuscarinic agents were evaluated through the 30 models available in TOPKAT toxicity evaluation software.[24] Out of these 30 models, only rat oral LD_{50} values of the compounds showed modest correlations with inhibition of [3H]NMS binding of N4TG1 muscarinic receptors. A negative linear trend was observed when rat oral LD_{50} values (Table 3) were plotted against the log K_i for

Figure 12. MEP profiles (calculated at B3LYP/6-31G** level) of atropine (left) and protonated atropine (right) beyond Van der Waals surface. (Top row): at −20.0 kcal/mol; (Middle row): at −10.0 kcal/mol; (Bottom row): at −5.0 kcal/mol.
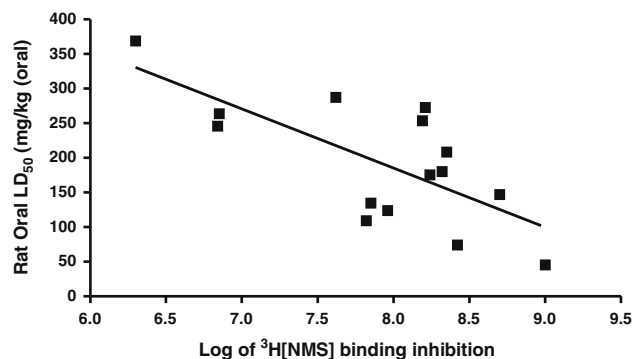
Figure 13. A linear relationship established between log 3H[NMS] binding inhibition (x-axis) and rat oral LD_{50} (y-axis).

[3H]NMS binding and log IC_{50} values of α-amylase release. The correlation between pK_i for inhibition of [3H]NMS binding and rat oral LD_{50} yielded a linear equation with a weak correlation coefficient 0.61 (Fig. 13, Table 3). The correlation between rat oral LD_{50} and α-amylase log IC_{50} followed a similar negative linear trend with a correlation coefficient = 0.56. No correlation was observed with data obtained from inhibition of guinea pig ileum contraction. Experimental LD_{50} of atropine was about 500 mg/kg (oral) in mouse. Taken together, the 2,2-diphenylpropionates are predicted to exhibit somewhat greater toxicity than atropine.

2.7. Pharmacophore model for antimuscarinic activity

We have developed a 3D pharmacophore model for antimuscarinic activity of the 15 2,2-diphenylpropionate compounds using the CATALYST 4.10 software.[25] The algorithm treats molecular structures as templates comprising of chemical functions localized in space that will bind effectively with complementary functions on the respective binding proteins. The most relevant biological features are extracted from a small set of compounds that cover a broad range of activity. It enables the use of structure and activity data for a set of lead compounds to generate a pharmacophore characterizing the activity of the lead set. We have used the HypoGen algorithm that allows identification of pharmacophores that are common to the 'active' molecules in the training set but are absent in the 'inactives'.[26] Structures of the 15 α-substituted 2,2-diphenylpropionate antimuscarinic agents for the training set were either built from the fragments or imported into CATALYST from other directories and energy minimized to the closest local minimum using the generalized CHARMM-like force field as implemented in the program. The 'best searching procedure' was applied to select representative conformers within 20 kcal/mol from the global minimum.[25] The automatic generation procedure using the HypoGen algorithm in CATALYST was adopted for generation of the pharmacophore, setting the default parameters as described in the method section. The pharmacophore is then used to estimate the activities of the training set. A plot of the experimental and predicted activity values (Table 5) is shown in Figure 14. The pharmacophore generated from the above training set of substituted diphenylpropionates was found to contain an aromatic ring and a hydrogen bond donor and likely a cationic nitrogen species roughly at a distance of 4 Å from the hydrogen bond acceptor. The pharmacophore and its mapping on selected compounds of the training set and protonated atropine are shown in Figure 15. The mapping of the pharmacophore on neutral atropine is shown in Figure 16. Both the neutral and protonated form of atropine appear to share the aromatic ring and a hydrogen bond donor features. Significantly, the pharmacophore characterized by these two features is also statistically found to be the most relevant pharmacophore by the sta-
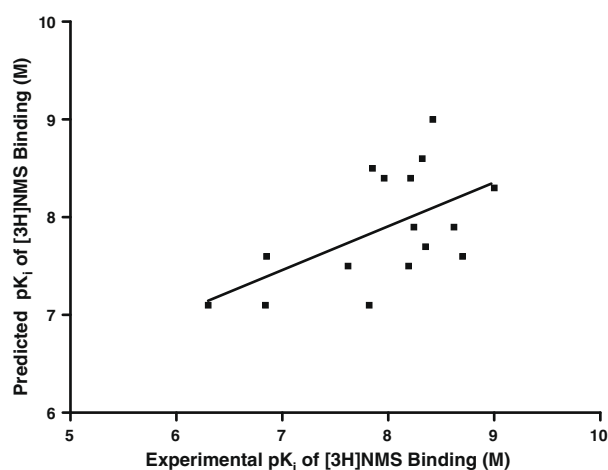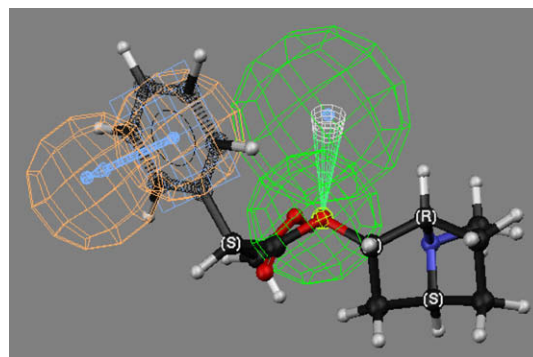
Table 5
Comparative data of the experimental versus predicted activity values (using the generated pharmacophore model)

Compound#	Experimental [³H] NMS binding, pK_i (M)	Predicted [³H] NMS binding, pK_i (M)	Error[a]
1	6.3 ± 0.03	7.1	1.1
2	6.8 ± 0.06	7.6	1.1
3	7.8 ± 0.04	8.5	1.1
4	8.2 ± 0.04	7.5	−1.1
5	8.2 ± 0.02	7.9	−1.0
6	8.4 ± 0.02	9.0	1.1
7	8.2 ± 0.02	8.4	1.0
8	7.8 ± 0.03	7.1	−1.1
9	8.3 ± 0.06	7.7	−1.1
10	8.0 ± 0.06	8.4	1.1
11	8.8 ± 0.04	7.6	−1.1
12	9.0 ± 0.04	8.3	−1.1
13	8.3 ± 0.04	8.6	1.0
14	7.7 ± 0.02	7.5	−1.1
15	6.9 ± 0.06	7.1	1.0
Atropine	8.7 ± 0.08	7.9	−1.1

[a] Values in the error column represent the ratio of estimated activity to experimental activity, or its negative inverse if the ratio is less than one.

Figure 14. Correlation between experimental versus predicted activity values (using the generated pharmacophore model).

Figure 16. Pharmacophore mapping on neutral atropine.

tistical CatScramble evaluations.[25] The predicted activity values along with the experimentally determined values of the compounds are presented in Table 5. Although a plot of experimental and predicted activity values of the compounds in the training set in CATALYST demonstrated a good correlation ($R = 0.89$), the values are not well distributed over the graph due to close proximity of the experimental activity values (not shown). Nonetheless, this pharmacophore is our starting model that allowed us to identify new potential antimuscarinic compounds through virtual screening of our in-house CIS database.[27]

Based on the above derived pharmacophore model, we chose 10 candidate compounds as a first test set in our biological assay to evaluate the potential power of the pharmacophore based search of the in-house 3D CIS database. It contains over 290,000 compounds, and the CIS database is not composed of atropine analogs (or muscarinic antagonists in general). The inhibition potency in our biological assay and structure of the 10 identified compounds together with atropine (**2′**) are reported in Chart 2. The 10 compounds are 1-ethyl-1-(2-(3-hydroxy-2-phenylpropanoyloxy)ethyl)piperidinium, **1′**, (BL58125); 2-(diethylamino)ethyl 2,2-diphenylpropanoate, **3′**, (ZW62841); 1-methylpiperidin-4-yl 3-hydroxy-2-(4-(trifluoromethyl)phenyl)propanoate, **4′**, (BL13260); 4-cyclopentyl-4-hydroxy-N,N,N-trimethyl-4-(thiophen-2-yl)but-2-yn-1-aminium, **5′**, (AE08907); 2-(2,2-diphenylacetoxy)-N,N,N-trimethylethanaminium, **6′**, (AB39 587); 1-(3-(dimethylamino)propyl)piperidin-4-yl 2-hydroxy-2,2-
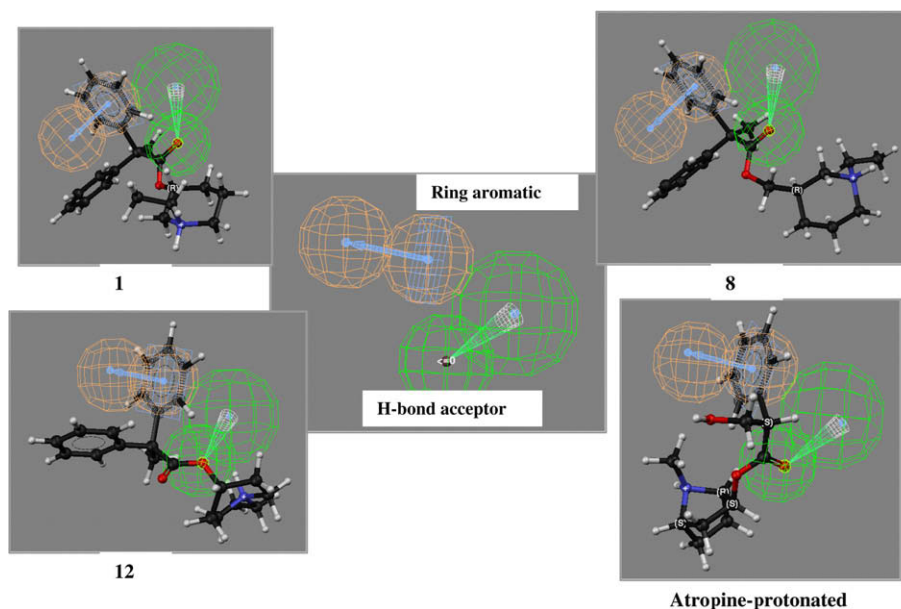
Figure 15. Pharmacophore (middle) and its mapping on **1**, **8**, **12**, and atropine-protonated.
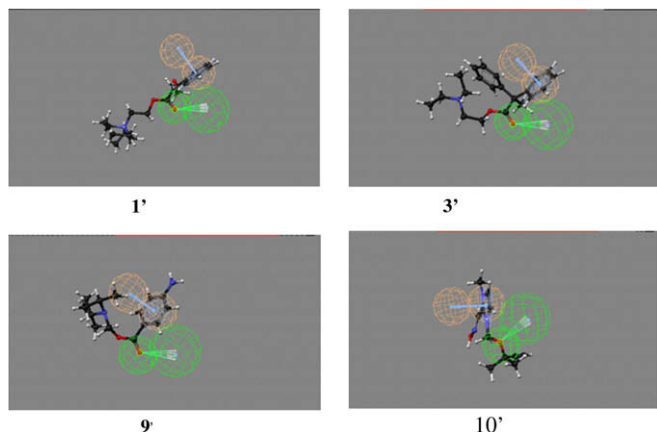
Figure 17. Mapping of the pharmacophore onto the four identified candidate mAChR inhibitors obtained by searching our in-house database.

diphenylacetate, **7′**, (AF70711); 4-(2-(benzoyloxy)propan-2-yl)-3-methylthiazol-3-ium, **8′**, (AJ78856); (diisopropylamino) methyl 4-aminobenzoate, **9′**, (AE04963); 2-((hydroxyimino) methyl)-1-methyl-3-(*tert*-pentyloxymethyl)-1*H*-imidazol-3-ium (*Z*-isomer), **10′**, (BL09220); and 2-(3,4-dichlorophenylamino)-*N*,*N*-diethyl-*N*-methyl-2-oxoethanaminium, **11′**, (AS67031).

Two of 10 compounds, **1′** and **3′** were found to be close in activity to atropine (**2′**) and five of the compounds were found to have antimuscarinic activity less than 200 nM and have not been reported as antimuscarinics (Chart 2). While all 10 compounds mapped onto the pharmacophore model, mappings of the two more potent and two less potent structures are shown in Figure 17, where it is clear that the more active inhibitors superimpose the ring aromatic and the hydrogen bond acceptor (**1′** and **3′**). In contrast, the structures exhibiting weak inhibition (**9′** and **10′**) have moieties that intrude into the ring aromatic (**10′**) or hydrogen bond acceptor (**9′**). The mapping of these identified compounds demonstrates the potential power of the pharmacophore model. It is important to note that although the directed approach of 3D database search is an efficient tool for extracting potential bioactive compounds, it is necessary to experimentally test the compounds and iteratively refine the model. Also, despite good mapping fit of a particular molecule to the pharmacophore model reflecting receptor complementarity, its experimental activity is not guaranteed.[26] There may be several factors lacking, such as the perfect fit to the active site due to steric hindrance, electrostatics, overall lipophilicity, and other unforeseen parameters. Thus, in our study, despite reasonably well mapping of the pharmacophore model onto the 10 compounds, not all the compounds were found to have similar inhibition potency. Nonetheless, the model provided the foundation for identification of such compounds that will eventually allow us to develop a robust test set of antimuscarinic agents. We are continuing to refine the model to provide more accurate information about the exact feature requirements for antimuscarinic activity in general and, perhaps, subtype specificity in particular. The currently fielded antimuscarinic to protect against chemical warfare agents (organophosphates) that irreversibly poison acetylcholinesterase and cause a cholinergic crisis in man is atropine.[28] However, atropine exhibits similar binding affinities to all of the five known muscarinic receptor subtypes. Atropine is a tertiary amine that competitively inhibits acetylcholine at postganglionic muscarinic sites, is rapidly absorbed following oral administration, and distributes to all tissues including the central nervous system, that is, atropine exhibits good pharmacokinetic properties for peripheral and central muscarinic receptors. Primary targets affected by atropine include heart, salivary glands,
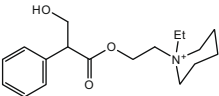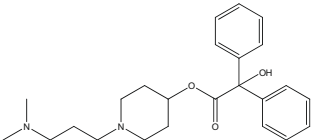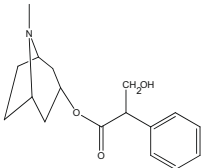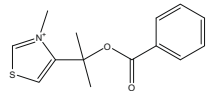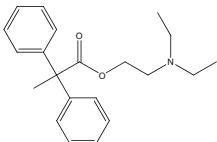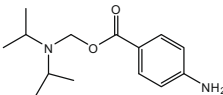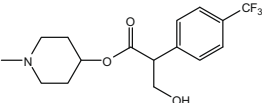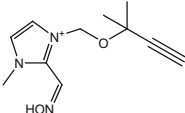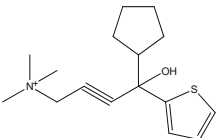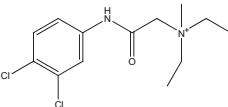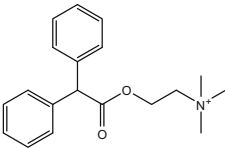
smooth muscle (gastrointestinal tract), central nervous system, as well as the eye. The observation that the M3 muscarinic receptor modulates the iris provides us with the hypothesis that we can select for antimuscarinic antagonists that lack or is minimized toward the M3 receptor while retaining M1 and M2 subtype selectivity for heart and neuronal therapy. In this manner, using our general pharmacophore model to select for novel antimuscarinics first, our second step will be to develop a subtype differentiating in silico pharmacophore model that could provide the means to reduced selectivity for M3 receptors and thereby reducing or eliminating mydriatic effects (pupil dilation). Thus, efficacy data of known compounds from published literature to derive a reliable 3D pharmacophore specific to these receptor subtypes could yield a 3D pharmacophore, which can be validated using ab initio quantum chemical calculations of many properties, including stereo-electronic, electric field, lipophilicity, and aromatic hydrophobic functions as described and documented in this paper for non-selective muscarinic antagonists. As in any model, reiterative processes of in silico modeling and evaluation[26] will refine the pharmacophore model to be more accurate within the selective criteria (e.g., muscarinic antagonist potency or receptor selectivity). Our basic model successfully provided predictive compounds of increased affinity for the muscarinic receptor.

3. Conclusions

The present QSAR study on the calculated stereo-electronic properties of 15 muscarinic antagonists provided valuable molecular level information and insights about the antimuscarinic activity of α-substituted 2,2-diphenylpropionates. The non-bonded distance between the carbonyl oxygen and the protonated nitrogen atom of the heterocyclic ring and the torsion angle between the aromatic ring plane and heterocyclic ring were found to be important structural components for potent antimuscarinic activity of the compounds.

An aqueous environment was calculated to be important for antimuscarinic activity. However, the stretching vibration frequencies of the ether oxygen and the carbonyl group were determined to have a more important role for the antimuscarinic activity of the compounds. In terms of electronic properties, reactivity indexes, specific location MEP potentials, HOMO and LUMO isodensity surface, all were found to have a distinct relationship with activity. Nucleophilic affinity of the nitrogen in the heterocyclic ring and hydrophobicity of the aromatic moieties appear to play a significant electronic role toward antimuscarinic activity. The 3D pharmacophore model for antimuscarinic activity containing an aromatic ring and a hydrogen bond acceptor is consistent with this observation. The resulting pharmacophore allowed us to identify several potential antimuscarinic compounds through virtual screening of an in-house database, from which we have chosen 10 candidate compounds for evaluation in the [³H]NMS biological assay for antimuscarinic inhibition potency. Eight of the compounds showed 2–200 nM inhibition of ligand binding (two about equal in inhibition potency to atropine) and none were previously reported as antimuscarinics.

In summary, the above described calculated results should aid in the rational design of more efficacious antimuscarinic drugs, in particular, specific assays containing only mAChR subtype should lead to a muscarinic receptor subtype pharmacophore and more potent subtype specific inhibitors. Optimization of calculated structural parameters: (a) the stretching frequency of the ether oxygen atom, (b) the carbonyl stretching vibrations, (c) enhancing the reactivity indexes, and (d) compounds with specific locations of hydrogen bond acceptor and hydrophobic characteristics should provide potent antimuscarinic compounds. These quantitative

#	Structure	pK$_i$ (M)	#	Structure	pK$_i$ (M)
1'		8.7 ± 0.24	7'		6.8 ± 0.01
2'		8.4 ± 0.41	8'		5.5 ± 0.08
3'		8.2 ± 0.01	9'		5.3 ± 0.07
4'		7.7 ± 0.16	10'		4.5 ± 0.57
5'		7.1 ± 0.10	11'		>3.33
6'		7.1 ± 0.36			

Chart 2. Structures of the 10 newly identified antimuscarinic agents and atropine along with their experimental efficacy data. (Compound numbers are indicated as #.)

structure–activity relationship studies derived from correlations between experimental activity and theoretical parameters of the compounds provided a better understanding of the requirement for efficacious therapeutics.

4. Experimental

4.1. Procedure followed for quantum chemical calculations

Conformation search calculations using the 'systematic search' technique via single-point AM1 method in SPARTAN[29] was used to generate different conformers for each of the molecules. The minimum energy conformer with highest abundance (a Boltzmann population density greater than 70.0%) was chosen for full geometry optimization using the AM1 algorithm[21] followed by re-optimizations at ab initio quantum chemical level of computations using the GAUSSIAN 98 package.[22] Geometry optimizations were carried out sequentially at increasing levels of theory or basis sets as inputs starting from the AM1 optimized geometry on the singlet states of neutral molecules. Hybrid B3LYP/6-31G** functional was found to be the optimum choice for calculations of this size of molecules, with an average molecular weight of 300 Da.[30] The computations were carried out on a Silicon Graphics Octane workstation.

In order to simulate physiological conditions, complete geometry optimization of the molecules was performed in the presence of an aqueous environment using the AM1 aq method developed by Dixon et al.[31] in SPARTAN and subsequently, single point calculations using the ab initio polarizable continuum model (SCRF = PCM).[32] Molecular electronic properties such as molecular orbital energies, electrostatic potentials, atomic charges, proton affinities, octanol–water partition coefficients (log *P*), and other structural parameters were calculated on the optimized geometry of each of the molecules as implemented in the above software.

Molecular electrostatic potential (MEP) maps and molecular electronic profiles such as molecular orbital isosurfaces were generated and sampled over the entire accessible surface of a molecule (corresponding roughly to a van der Waals contact surface) using the graphics of SPARTAN.[29] The MEP maps provide a measure of charge distribution from the point of view of an approaching reagent.

4.2. Procedure for generation of the 3D pharmacophore model

A three-dimensional pharmacophore was developed using the CATALYST 4.10 methodology.[25] This is an integrated commercially available software package (Accelrys Inc. CA) that generates pharmacophores, commonly referred to as 'hypotheses' in the CATALYST terminology. It enables the use of structure and activity data for a set of lead compounds to create a 'hypothesis', thus characterizing the activity of the lead set. At the heart of the software is the HypoGen algorithm that allows identification of 'hypotheses' that are common to the 'active' molecules in the training set but at the same time not present in the 'inactives'.[26] A training set with 15 α-substituted 2,2-diphenylpropionate antimuscarinic agents[3] including atropine was created and conformational models of the training set were generated that emphasize representative coverage within a range of the permissible Boltzmann population with significant abundance (within 10.0 kcal/mol) of the calculated global minimum. This selected conformational model was used for pharmacophore generation within CATALYST, which aims to identify the best three-dimensional arrangement of chemical functions such as hydrophobic regions, hydrogen bond donor, hydrogen bond acceptor, and positively and/or negatively ionizable sites distributed over a three dimensional space explaining the activity variations among the training set. The hydrogen bonding features are vectors, whereas all other functions are points. Pharmacophore generation was carried out with the above mentioned 15 α-substituted 2,2-diphenylpropionates (Chart 1) by setting the default parameters in the automatic generation procedure in CATALYST such as function weight 0.302; mapping coefficient, 0; resolution, 287 pm, and activity uncertainty 3. Default values were found to provide better initial estimation of experimental activities for these compounds. An uncertainty 'Δ' in the CATALYST paradigm indicates an activity value lying somewhere in the interval from 'activity divided by Δ' to 'activity multiplied by Δ'. Hypotheses approximating the pharmacophore of the α-substituted 2,2-diphenylpropionates are described as a set of aromatic hydrophobic, hydrogen bond acceptor, hydrogen bond acceptor lipid, positively and negatively ionizable sites distributed within a 3D space. The statistical relevance of various generated hypotheses is assessed on the basis of the cost relative to the null hypothesis and the correlation coefficients. The hypotheses are then used to estimate the activities of the training set. These activities are derived from the best conformation generation mode of the conformers displaying the smallest root-mean square (RMS) deviations when projected onto the hypothesis. HypoGen considers a pharmacophore that contain features with equal weights and tolerances. Each feature (e.g., hydrogen-bond acceptor, hydrogen-bond donor, hydrophobic, positive ionizable group, etc.) contributes equally to estimate

the activity. Similarly, each chemical feature in the HypoGen pharmacophore requires a match to a corresponding ligand atom to be within the same distance (tolerance).[33] Thus, the two parameters of fit score and conformational energy costs are crucial for estimation of predicted activity of the compounds. The method has been documented to perform better than a structure-based pharmacophore generation.[18,34]

The statistical relevance of the obtained pharmacophore is assessed on the basis of the cost relative to the null hypothesis and the correlation coefficient along with CatScrambled confidence level of the pharmacophore.[25] The pharmacophore is then used to estimate the activities of the training set. To obtain a good model which adequately describes the interaction of ligands with high predictability, a collection of 15–20 compounds of different chemical classes with a broad range biological activity has been recommended.

The pharmacophore developed in this study was used as a template to search an in-house Chemical Information System (CIS) database[27] for new compounds not yet evaluated for antimuscarinic activity. The CIS database has over 290,000 compounds, mostly exhibiting antimalarial or antileishmanial activities. The structures of each of the CIS database compounds were transformed into all conformations ranging from 0 to 20 kcal/mol and stored into a multiconformer form by using the catDB utility program of CATALYST software.[25] The catDB format allows a molecule to be represented by a limited set of conformations, thereby permitting conformational flexibility to be included during the search of the database.

4.3. Compound selection after database search

The pharmacophore mapped on one of the potent inhibitors was converted into a shape-based 3D template to account for the steric factors associated with the binding. This template was used to search the CIS-WRAIR. The down selection of the identified compounds was carried out by evaluating the in silico ADME/Toxicity properties and choosing only those compounds that were favorable for blood-brain barrier penetration lipophilicity, and rat oral LD_{50} properties. In silico ADME/Toxicity of the α-substituted 2,2-diphenylpropionate antimuscarinic agents were evaluated through 30 models available in TOPKAT[24] toxicity evaluation software and by CERIUS2 software[35] for blood-brain partition. The overall procedure of compound identification and selection was carried out in an iterative manner by generating several shape-based pharmacophore templates on selected potent α-substituted 2,2-diphenylpropionates. Ultimately, we were able to down select 25 compounds to be assayed for potential antimuscarinic activity.

4.4. Chemistry

The compounds used in the paper were taken from earlier published literature; their characteristics are summarized below:

The 2,2-diphenylpropionates have been synthesized by reacting the 2,2-diphenylpropionyl chloride with the corresponding amino alcohol.[3] For biological experiments, free bases were dissolved in 0.01 M hydrochloric acid, and these solutions were diluted as required. Azabicylco diphenylpropionates were synthesized as reported in the literature.[3,36]

The 10 newly identified antimuscarinic agents were obtained on contract from the WRAIR-CIS.[27] Data sheets for these 10 compounds (Table 2) (BL58125, ZW62841, BL13260, AE08907, AB39587, AF70711, AJ78856, AE04963, BL09220, and AS67031 are available from Ref. 27.

4.4.1. Structure confirmation of the 10 identified compounds

The ^1H NMR spectra of compounds **3′–11′** were obtained using a Bruker Advance 300 or 600 MHz NMR spectrometer, and these

spectra are included in the Supplementary data. The ^{1}H NMR spectrum of compound **1** was obtained using a 90 MHz NMR spectrometer (data provided by CIS database, Rockville, MD).[27]

4.4.1.1. 1-Ethyl-1-(2-(3-hydroxy-2-phenylpropanoyloxy)ethyl) piperidinium (1′).
^{1}H NMR (DMSO-d_6) 1.11 (t, 3H, –CH$_2$C*H$_3$*), 1.70 (m, 5H, C*H$_2$s* piperidine), 3.32–4.00 (m, 9H, C*H$_2$s* piperidine, –C*H$_2$*CH$_3$, –CO$_2$C*H$_2$*CH$_2$–, C*H*), 4.44 (m, 4H, –C*H$_2$*OH, –CO$_2$C*H$_2$*CH$_2$), 7.31 (s, 5H, C$_6$*H$_5$*). Non-hygroscopic, mp = 109–111 °C, solubility = water, methanol, ethanol, and DMSO-d_6.

4.4.1.2. 2-(Diethylamino)ethyl-2,2-dicyclohexylpropanoate (3′).
^{1}H NMR (D$_2$O) 1.04 (m, 6H, –NCH$_2$C*H$_3$*), 1.95 (m, 4H, –NC*H$_2$*CH$_3$), 2.92 (m, 4H, C*H$_3$*CH(Ph)$_2$), 3.40 (m, 2H, C*H$_2$*N(Et)$_2$), 4.47 (m, 2H, COOC*H$_2$*), 7.24–7.35 (m, 10H, C$_6$*H$_5$*). Non-hygroscopic, mp = 163 °C, solubility = water, moderately in ethanol and acetone.

4.4.1.3. 1-Methylpiperdin-4-yl 3-hydroxy-2-(4-(trifluromethyl) phenyl)propanoate (4′).
^{1}H NMR (D$_2$O) 1.76–2.23 (m, 4H, C*H$_2$* piperidine), 2.68–3.51 (m, 5H, C*H$_2$* piperidine, C*H$_3$*), 3.92–4.18 (m, –C*H*C*H$_2$*–OH), 4.98 (br s, C*H*, 0.3H), 5.12 (br s, C*H*, 0.7H), 7.55–7.71 (m, 4H, Ph). Non-hygroscopic, stable in acid, heat and light, unstable in base, mp = 161–162 °C, solubility = water and acids, moderately in methanol and acetone.

4.4.1.4. 4-Cyclopentyl-4-hydroxy-N,N,N-trimethyl-4-(thiophen-2-yl)but-2-yn-1-aminium (5′).
^{1}H NMR (CDCl$_3$) 1.26 (s, 3H, C*H$_3$*), 1.44–1.62 (m, 10H, cyclopentyl C*H*s, alkyne C*H*), 2.37 (s, 6H, 2C*H$_3$*), 2.52 (t, 1H, alkyne C*H*)*, 3.50 (s, 2H, C*H$_2$*)*, 6.96 (d, 1H, thiophene C*H*), 7.19 (s, 1H, thiophene C*H*). *COSY NMR was used to determine that there was a correlation between these protons on adjacent carbons. Remaining thiophene CH was overlapped by solvent peak at 7.27 ppm. Also, ^{1}H NMR in DMSO-d_6 is included in the Supplementary data. Non-hygroscopic, stable in light, mp = not available, solubility in water.

4.4.1.5. 2-(2,2-Diphenylacetoxy)-N,N,N-trimethylethanaminium (6′).
^{1}H NMR (D$_2$O) 2.83 (s, 9H, –N$^+$C*H$_3$*), 3.51 (m, 2H, C*H$_2$*), 4.49 (m, 2H, C*H$_2$*), 5.22 (s, 1H, C*H*), 7.26–7.31 (m, 10H, C$_6$*H$_5$*). Non-hygroscopic, stable in light, mp = 198–199.5 °C, solubility = water, moderately in ethanol and chloroform.

4.4.1.6. 1-(3-(Dimethylamino)propyl)piperidin-4-yl 2-hydroxy-2,2-diphenylacetate (7′).
^{1}H NMR (D$_2$O) 2.05 (br s, 6H, C*H$_3$* piperidine), 2.47 (br s, 2H, C*H$_2$* propyl), 2.81 (s, 6H, –N(C*H$_3$*)$_2$), 2.92 (br s, 2H, C*H$_2$* propyl), 3.13 (t, 4H, C*H$_2$* piperidine), 3.29 (br s, 2H, C*H$_2$* propyl), 5.24 (br s, 1H, C*H* piperidine), 7.38–7.42 (m, 10H, C$_6$*H$_5$*). Non-hygroscopic, stable in light, unstable in base, mp = not available, solubility = water.

4.4.1.7. 4-2-(Benzoyloxy)propan-2-yl)-3-methylthiazol-3-ium (8′).
^{1}H NMR (DMSO-d_6) 1.99 (s, 6H, 2 C*H$_3$*s), 4.17 (s, 3H, C*H$_3$*), 7.57 (t, 2H, Ph Hs), 7.72 (t, 1H, Ph H), 8.00 (d, 2H, Ph Hs), 8.26 (d, 1H, C*H*), 10.10 (s, ~1H, C*H*). Yellow crystalline solid, mp = 179–181 °C, solubility = water.

4.4.1.8. (Diisopropylamino)methyl 4-aminobenzoate (9′).
^{1}H NMR (D$_2$O) 1.33 (s, 12H, –NCH(C*H$_3$*)$_2$), 3.53 (t, 2H, N*H$_2$*), 3.74 (m, 2H, C*H*), 4.51 (t, 2H, C*H$_2$*), 6.76 (d, 2H, Ph Hs), 7.77 (d, 2H, Ph Hs). Non-hygroscopic, stable in light, mp = not available, solubility = water.

4.4.1.9. (E/Z)-2-((Hydroxyimino)methyl)-1-methyl-3-((2-methylbut-3-yn-2-yloxy)methyl)-1H-imidazol-3-ium (10′).
^{1}H NMR (DMSO-d_6) 1.45 (s, 6H, 2C*H$_3$*s), 3.60 (s, 1H, alkyne C*H*), 3.96 s, 3H, C*H$_3$*-imidazole), 5.87 (s, 2H, C*H$_2$*-imidazole), 7.91 (s, 1H, imidazole),

7.99 (s, 1H, imidazole), 8.53 (s, 1H, C*H*, C*H*=NOH), 13.25 (s, 0.65H, O*H*). *Water peak and acetone peak also present in addition to solvent peak. Hygroscopic, stable in acid, heat and light, unstable in base, mp = 138–140 °C, solubility = water, acid and base, moderately in methanol and ethanol.

4.4.1.10. 2-(3,4-Dichlorophenylamino)-N,N-diethyl-N-methyl-2-oxoethanaminium (11′).
^{1}H NMR (D$_2$O) 1.33 (d, 6H, –CH$_2$C*H$_3$*), 3.17 (s, 3H, –NC*H$_3$*), 3.60 (t, 4H, C*H$_2$*CH$_3$), 4.14 (d, 2H, C*H$_2$*), 7.30 (d, 1H, Ph), 7.50 (d, 1H, Ph), 7.69 (s, 1H, Ph). Non-hygroscopic, stable in light, mp = not available, solubility = water.

4.5. Equilibrium binding assays for testing antimuscarinic activity of the down select compounds

Briefly, typical equilibrium binding assays (see Refs. 3 and 37) were performed in triplicate using ~107 μg of protein obtained from guinea pig brain and 2 nM of the ligand [^{3}H]*N*-methylscopolamine (Perkin Elmer, Norwalk CT); non-specific binding was determined using an excess of a cold ligand (100 μM atropine, Sigma–Aldrich, St Louis, MI). Reaction mixtures included protein, 50 mM potassium phosphate buffer (pH 7.4), test compound or buffer, atropine or buffer and the radioligand. After 60 min at room temperature, the assays were terminated by collecting the samples on glass-fiber filters with a cell harvester (Wallac Filtermat B, Perkin Elmer FilterMate Harvester, Perkin Elmer, Norwalk, CT). Starting concentration of the compounds was 0.1 mM for each assay which was subsequently diluted twofold 20 times. The filtermat was dried in a vacuum oven, and counted in a Perkin Elmer MicroBeta TriLux scintillation counter (Perkin Elmer, Norwalk, CT). Specific [^{3}H]ligand binding to receptors was determined by subtracting the total from the non-specific counts. The K_i values were derived from the IC$_{50}$ values by correcting for receptor occupancy by the [^{3}H]ligand; the K_D value determined for the [^{3}H]*N*-methylscopolamine is 0.48.[37] The binding parameters were obtained using non-linear analysis (Prism, GraphPad Software, V4, San Diego, CA).[37]

Supplementary data

Supplementary data associated with this article can be found, in the online version, at doi:10.1016/j.bmc.2009.04.001.

References and notes

1. Bakshi, K. S.; Pang, S. N. J.; Snyder, R. *J. Toxicol. Environ. Health A* **2000**, *59*, 282; Romano, J. A.; King, J. M. *Mil. Med.* **2001**, *166*, 21.
2. Marrs, T. C. *Pharmacol. Ther.* **1993**, *58*, 51.
3. Gordon, R. K.; Breuer, E.; Padilla, F. N.; Smejkal, R. M.; Chiang, P. K. *Mol. Pharmacol.* **1989**, *36*, 766.
4. Bajgar, J. *Adv. Clin. Chem.* **2004**, *38*, 151.
5. Patocka, J.; Kuca, K.; Jun, D. *Acta Med. (Hradec Kralove)* **2004**, *47*, 215.
6. Wess, J.; Eglen, R. M.; Gautam, D. *Nat. Drug Disc.* **2007**, *6*, 721.
7. Caulfield, M. P.; Birdsall, N. J. M. *Pharmacol. Rev.* **1998**, *50*, 279.

8. Taylor, P.; Brown, J. H. In *Goodman Gilman's The Pharmacological Basis of Therapeutics*; Brunton, L. L., Ed., 11th ed.; McGraw-Hill: New York, 2006. Chapter 7, pp 183–200.
9. Leader, H.; Wolfe, A. D.; Chiang, P. K.; Gordon, R. K. *J. Med. Chem.* **2002**, *45*, 902.
10. Tattersall, J. E. *Br. J. Pharmacol.* **1993**, *108*, 1006.
11. Loke, W. K.; Sim, M. K.; Go, M. L. *Eur. J. Pharmacol.* **2002**, *442*, 279.
12. Loke, W. K.; Sim, M. K.; Go, M. L. *Eur. J. Pharmacol.* **2005**, *521*, 59.
13. Shih, T.; Whalley, C. E.; Valdes, J. J. *Toxicol. Lett.* **1991**, *55*, 131.
14. Buchwald, P.; Bodor, N. *Drug Future* **2002**, *27*, 577.
15. Janseen, D. *Drug Disc.* **2002**, *38*, 1.
16. Podlogar, B. L.; Muegge, I.; Brice, L. J. *Curr. Opin. Drug Disc.* **2001**, *12*, 102.
17. Bhattacharjee, A. K. *Front. Drug Des. Disc.* **2007**, *3*, 257.
18. Bhattacharjee, A. K.; Hartell, M. G.; Nichols, D. A.; Hicks, R. P.; Stanton, B.; van Hamont, J. E.; Milhous, W. K. *Eur. J. Med. Chem.* **2004**, *39*, 59.
19. Bhattacharjee, A. K.; Geyer, J. A.; Woodard, C. L.; Kathcart, A. K.; Nichols, D. A.; Prigge, S. T.; Li, Z.; Mott, B. T.; Waters, N. C. *J. Med. Chem.* **2004**, *47*, 5418.
20. Ashani, Y.; Bhattacharjee, A. K.; Leader, H.; Saxena, A.; Hinrichs, C.; Doctor, B. P. *Biochem. Pharmacol.* **2003**, *66*, 191.
21. Dewar, M. J. S.; Zoebisch, E. G.; Horsley, E. F.; Stewart, J. J. P. *J. Am. Chem. Soc.* **1985**, *107*, 3902.
22. Frisch, M. J.; Trucks, G. W.; Schlegel, H. B.; Scuseria, G. E.; Robb, M. A.; Cheeseman, J. R.; Zakrzewski, V. G.; Montgomery, J. A.; Stratmann, R. E.; Burant, S. Dapprich, J. C.; Millam, J. M.; Daniels, A. D.; Kudin, K. N.; Strain, M. C.; Farkas, O.; Tomasi, J.; Barone, V.; Cossi, M.; Cammi, R.; Mennucci, B.; Pomelli, C.; Adamo, C.; Clifford, S.; Ochterski, J.; Petersson, G. A.; Ayala, P. Y.; Cui, Q.; Morokuma, K.; Malick, D. K.; Rabuck, A. D.; Raghavachari, K.; Foresman, J. B.; Cioslowski, J.; Ortiz, J. V.; Stefanov, B. B.; Liu, G.; Liashenko, A.; Piskorz, P.; Komaromi, I.; Gomperts, R.; Martin, R. L.; Fox, D. J.; Keith, T.; Al-Laham, M. A.; Peng, C. Y.; Nanayakkara, A.; Gonzalez, C.; Challacombe, M.; Gill, P. M. W.; Johnson, B. G.; Chen, W.; Wong, M. W.; Andres, J. L.; Head-Gordon, M.; Replogle, E. S.; Pople, J. A. GAUSSIAN *98 (Revision A.1)*; Gaussian: Pittsburgh, PA, 1998.
23. Cramer, C. J.; Truhlar, D. G.. In *Reviews in Computational Chemistry*; Lipkowitz, K. B., Boyd, D. B., Eds.; VCH: New York, 1995; Vol. 6, pp 1–172. Continuum Solvation Models: Classical and Quantum Mechanical Implementations.
24. TOPKAT *Version 6.2*; Accelrys: San Diego, CA, 2005.
25. CATALYST *Version 4.10*; Accelrys: San Diego, CA, 1998.
26. Gunner, O.A. In: *Pharmacophore, Perception, Development, and Use in Drug Design*; University International Line: San Diego, 2000, pp 17–20.
27. Chemical Information System; Division of Experimental Therapeutics, Walter Reed Army Institute of Research, Silver Spring, MD, USA. Archives of the Chemical Information System, Division of Experimental Therapeutics, Washington, DC; Data Sheet #: BL58125; ZW62841; BL13260; AE08907; AB39587; AF70711; AJ78856; AE04963; BL09220; AS67031.
28. Newmark, J. *Arch. Neurol.* **2004**, *61*, 649.
29. SPARTAN *Version 5.1*; Wavefunction, 18401 Von Karman Ave., #370, Irvine, CA 92715.
30. Koch, W.; Holthausen, C. *A Chemist's Guide to Density Functional Theory*; Wiley-VCH: Weinheim, Germany, 2000.
31. Dixon, R. W.; Leonard, J. M.; Hehre, W. J. A. *Israel J. Chem.* **1993**, *33*, 427.
32. Tomasi, J.; Cammi, R.; Mennucci, B. *Int. J. Quantum Chem.* **1999**, *75*, 767.
33. Greenidge, P. A.; Weiser, J. A. *Mini-Rev. Med. Chem.* **2001**, *1*, 79.
34. Grigorov, M.; Weber, J.; Tronchet, J. M.; Jefford, C. W.; Milhous, W. K. *J. Chem. Inf. Comput. Sci.* **1997**, *37*, 124.
35. CERIUS2 *Version* 4.9; Accelrys: San Diego, CA, 2003.
36. Carrol, F. I.; Abraham, P.; Parham, K.; Griffith, R. C.; Ahmad, A.; Richard, M. M.; Padilla, F. N.; Witkin, J. M.; Chiang, P. K. *J. Med. Chem.* **1987**, *30*, 805.
37. Gordon, R. K.; Nigam, S. V.; Weitz, J. A.; Dave, J. R.; Doctor, B. P.; Ved, H. S. *J. Appl. Toxicol.* **2001**, *21*, S47.